Photo-initiated crosslinking of a methacrylate/ionic liquid based gel polymer electrolyte: effect of the curing sequence on the electrochemical properties

H Porthault, G Piana, M Cesbron, V Armel, A Bazin, S Franger, S Oukassi

▶ **To cite this version:**

H Porthault, G Piana, M Cesbron, V Armel, A Bazin, et al.. Photo-initiated crosslinking of a methacrylate/ionic liquid based gel polymer electrolyte: effect of the curing sequence on the electrochemical properties. 2020. hal-02869973

HAL Id: hal-02869973

https://hal.science/hal-02869973v1

Preprint submitted on 16 Jun 2020

HAL is a multi-disciplinary open access archive for the deposit and dissemination of scientific research documents, whether they are published or not. The documents may come from teaching and research institutions in France or abroad, or from public or private research centers.

L'archive ouverte pluridisciplinaire **HAL**, est destinée au dépôt et à la diffusion de documents scientifiques de niveau recherche, publiés ou non, émanant des établissements d'enseignement et de recherche français ou étrangers, des laboratoires publics ou privés.

Photo-initiated crosslinking of a methacrylate/ionic liquid based gel polymer electrolyte: effect of the curing sequence on the electrochemical properties

H. Porthault[a], G. Piana[a,b], M. Cesbron[a], V. Armel[a], A. Bazin[a], S. Franger[b], S. Oukassi[a]

[a] *Univ. Grenoble Alpes, CEA, LETI, MINATEC Campus, 38054 Grenoble, France*

[b] *Universite Paris-Sud XI, Institut de Chimie Moléculaire et des Matériaux d'Orsay, Orsay, France*

**corresponding author: H. Porthault*

For Table of Contents use only

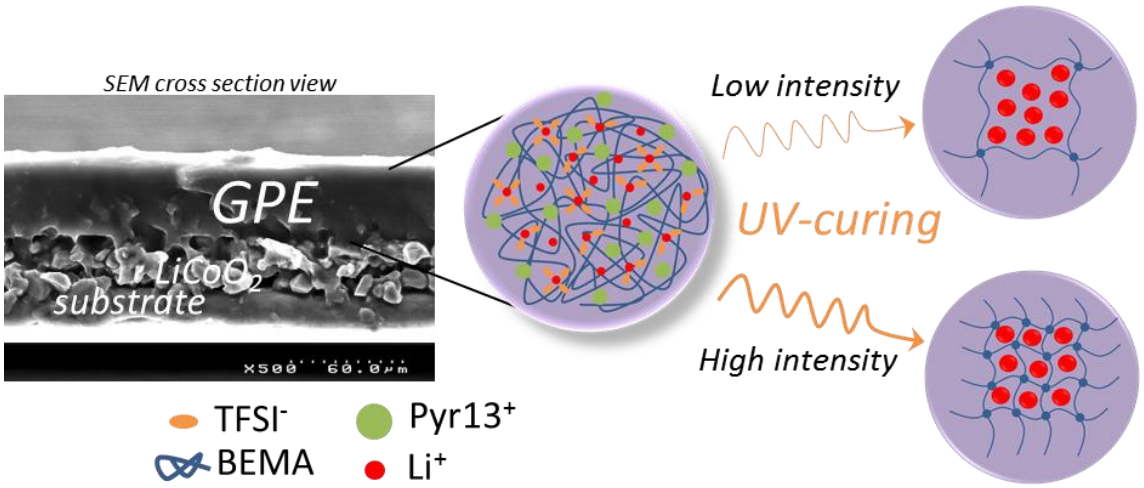

Abstract

In the present work, emphasis is given to the effect of the photo-curing sequence on the electrochemical properties of a methacrylate/ionic liquid based gel polymer electrolyte (GPE). The reaction mixture consists of BEMA (30 wt.%), LiTFSI (18 wt.%), PYR13TFSI ionic liquid (52 wt.%) using Darocur®1173 as photoinitiator. In-situ photo-DSC analyses show that the radiation intensity has no effect on the final conversion rate (100 % in all cases), whereas it considerably influences the polymerization rate and the final GPE structure. Namely, the obtained GPE mechanical strength increases with the radiation intensity (from 82 to 182kPa). For the same initial precursor solution, the GPE cured with the lower radiation intensity presents the highest ionic conductivity (up to + 40 %, 0.8 mS cm-1 at 25 °C). The temperature dependence of the ionic conductivity exhibits a VTF behavior for all considered crosslinking conditions. Particular attention is given to the investigation of the transport properties in the GPE using diffusion measurements by Nuclear Magnetic Resonance spectroscopy (PFG-NMR). It is found that for the same initial precursor solution, the lower radiation intensities tend to provide low crosslinking density polymers with longer chains which lead to an ionic conductivity increase.

Keywords

Lithium metal batteries, Gel polymer electrolytes, photo-initiated reticulation, ionic liquids, ion transport, PFG-NMR, thermal properties.

1. Introduction

Numerous accidents involving batteries have been reported over the last decade, from smartphone explosion to thermal runaway of automotive battery pack. Consequently, many studies are carried out to improve batteries safety. One of the main line of research is to substitute the classical liquid electrolyte, which suffers from potential leakage and high flammable properties, with a solid one. Within this context, lithium polymer batteries are studied since the 1970's with the solid polymer electrolyte (SPE) described by Armand *et al.*[1-3] composed of a solid polymer matrix of crystalline poly(ethylene) oxide (PEO) and a lithium salt. SPE greatly increases mechanical strength and safety. Nevertheless, despite numerous studies on host polymers, the main drawback remains the low ionic conductivity at room temperature (10^{-7}-10^{-4} S cm^{-1})[4-8] partly attributed to the PEO crystallinity. Subsequently, in 1975, an interesting route to increase ionic conductivity was proposed by Feuillade *et al.*[9] who trapped a liquid electrolyte in the host polymer network, where the ionic conductivity can be achieved through the liquid phase in addition to the host polymer[10-12]. The main feature of the polymer matrix is then its ability to trap the liquid electrolyte rather than its amorphous and conductive character. In some cases, the liquid electrolyte can also act as a plasticizer for the host polymer[13-14] increasing the ionic conductivity by decreasing the polymer crystallinity. Added liquids were at first standard carbonate-based electrolytes[12] but the obtained GPE presented lower safety compared to SPE. From the 2000's, many groups started to use ionic liquids as solvent because of their low vapor pressure and high thermal stability[15-17]. Ionic conductivity around 1 mS cm^{-1} can be achieved with these ternary electrolytes. In most studies, the GPE is a physical gel formed by solvent evaporation and where the host polymer chains (usually PEO or PVdF derivatives) are tied by weak Van der

Waals and hydrogen bonds. Limited mechanical strength is reported especially for GPE with high liquid contents. On the other hand, a crosslinked host polymer creating covalent bonds forms a chemical gel and both mechanical and liquid retention abilities of the GPE are improved[18]. Crosslinking is usually achieved by thermal curing[19-20] but few studies report photo-initiated processes[21-24]. Photo-initiated crosslinking displays major advantages, such as high spatial resolution[25], solvent-free systems, accurate polymerization control[26], very high crosslinking rates and low thermal budget (for polymerization or solvent drying). This technique is both economically and environmentally interesting for industrial processes[27]. In the literature, photo-initiated crosslinking is mainly carried out with organic methacrylate-based polymers like methyl methacrylate (MMA)[28-29], ethoxylated trimethylolpropane triacrylate (ETPTA)[30-31], bisphenol A ethoxylate dimethacrylate (BEMA)[32] or poly(ethylene glycol diacrylate) (PEGDA)[33]. In these examples, the crosslinking occurs through a free-radical mechanism composed of three main steps[34]: the initiation, the propagation and the termination (by combination or disproportionation). One of the most reported photo-initiators is the 2-hydroxy-2-methyl-1-phenyl-1-propanone (HMPP or Darocur®1173)[30, 35-36]. In most studies, GPE properties are tailored by varying the polymer network[32, 35, 37-38], nature and content of solvent[33] and/or lithium salt[28, 39]. Moreover, mechanical properties and ionic conductivity have been improved by adding reinforcements like ceramic fillers, clays and mainly Al_2O_3 nanoparticles[30, 36]. To the best of our knowledge, no study reports the influence of the photo-curing sequence, especially the radiation intensity, on the electrochemical properties whereas it has been demonstrated that curing sequence influences the conversion rate and mechanical properties of the obtained crosslinked polymer[27, 40].

In this work, we report on the synthesis by UV-curing process of a methacrylate based GPE. The influence of the radiation intensity is evaluated in terms of mechanical strength and polymerization kinetics. The impact of the structural modifications on the lithium transport is then carefully estimated by electrochemical methods and PFG-NMR spectroscopy.

2. Experimental

2.1. Materials and samples preparation

Bisphenol A ethoxylate dimethacrylate (BEMA, M_n~1700, EO/phenol 15), Darocur® 1173 (97 %) and bis(trifluoromethane)sulfonimide lithium salt (LiTFSI, 99.95%) are purchased from Sigma Aldrich. N-propyl-N-methylpyrrolidinium bis(trifluoromethanesulfonyl)imide ($PYR_{13}TFSI$, 99.9 %) is purchased from Solvionic (Figure 1).

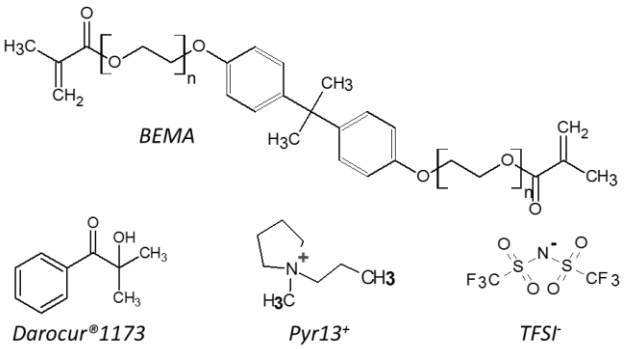

Figure 1: Chemical Structure of BEMA host polymer, Darocur1173 photo-initiator, Pyr_{13}^{+} cation and $TFSI^{-}$ anion.

The GPE electrolyte is composed of a binary liquid solution ($PYR_{13}TFSI$ and LiTFSI) and BEMA host polymer in a 70:30 wt.% ratio. Firstly, the liquid binary solution, consisting of LiTFSI dissolved in $PYR_{13}TFSI$, with a LiTFSI:$Pyr_{13}TFSI$ molar ratio of 0.3:1, is homogenized for 1 h by magnetic stirring. The BEMA monomer is then added to the solution and homogenized for 10 min. Still under stirring, 3 wt.% of the total solution weight of Darocur is added. After 5 min of homogenization, the solution is casted into a mold (depending on analyses) and

photo-cured with a mercury light source (centered around 365 nm) under various radiation intensities using UV filters. Depending on measurements, photo-curing is carried out with this source or directly in the characterization equipment (photo-DSC, etc.) with their proper UV-source. This explains why the reported radiation intensity values are not strictly the same from a characterization to another.

2.2 Conduction and Electrochemical measurements

Ionic conductivity is determined by electrochemical impedance spectroscopy (Biologic VMP3 multichannel galvanostat/potentiostat, frequency range : 100 mHz-1 MHz, ΔV = 10 mV) on coin cells composed of two stainless steel discs separated by a 200 µm- thick self-standing membrane of GPE polymerized at various radiation intensities. Measurements are done in a temperature controlled climatic chamber between 25 and 80 °C (298-353 K). The Nyquist plot did not display a semi-circle due to the presence of the ionic liquid, conferring a high ionic conductivity to the GPE. The Nyquist plots are fitted with a simple equivalent circuit model composed of a resistance (R) in series with a constant phase element (CPE) representing the blocking electrodes. The connections resistance being neglected, the high frequency resistance is considered as the electrolyte resistance.

The Pulsed-Field Gradient Nuclear Magnetic Resonance spectroscopy (PFG-NMR) is used to measure self-diffusion coefficients of each nucleus ^{7}Li, ^{1}H and ^{19}F, which reflect the diffusion of lithium, pyrrolidinium (Pyr) and TFSI molecules respectively[41-44]. All measurements are conducted with a Bruker AVANCE DSX spectrometer operating at 400 MHz with a Z-gradient direct detection broad-band probe. The GPE samples are directly polymerized in NMR tubes sealed under argon atmosphere. Considering the very low ^{7}Li transversal (spin-spin)

relaxation time (T_2) in the GPE, measurements are carried out at 60 °C to allow diffusion observation. NMR measurements of self-diffusion coefficients are conducted using a stimulated-echo sequence with bipolar gradient pulse pairs (supplementary file Figure S1). The signal intensity decay is fitted by equation 1 and the self-diffusion coefficient is determined by varying the gradient amplitude (G).

$$I = I_0 \exp\left[-(\gamma G \delta)^2 \left(\Delta - \frac{\delta}{3}\right) D\right] \qquad \text{(eq.1)}$$

Where I_0 is the signal intensity without applied gradient, γ is the gyromagnetic ratio, G the field gradient amplitude, δ the time of gradients application, Δ the diffusion delay ad D the self-diffusion coefficient.

The longitudinal relaxation time T_1, the time of RF 90° pulse P_1, the diffusion delay Δ and the gradient time application δ are optimized for each nucleus (supplementary file Table S1).

2.3 Morphological, thermal and mechanical characterizations

The surface morphology and thickness of the GPE are observed using a Hitachi 4000/4100 scanning electron microscope (SEM).

Differential Scanning Calorimetry (DSC) is carried out using a Q200 Model (TA Instruments). The samples are cooled at 10°C.min^{-1} down to -45 °C and then heated at 10 °C.min^{-1} up to 40 °C or 250 °C depending on materials. A Photo-Calorimeter Accessory (PCA, TA Instruments) (200 W high-pressure mercury source, 250-650 nm) coupled with DSC is used to characterize in-situ photo-curing reactions at various radiation intensities. Crosslinking kinetic parameters like conversion rate (C) and polymerization rate (R_p) are calculated according to the following equations:

$$C = \frac{\Delta H_t}{n \cdot m \cdot \Delta H_0} \quad \text{(eq.2)} \quad \text{and}$$

$$R_p = \frac{dC}{dt} = \frac{\frac{dH}{dt}}{n \cdot m \cdot \Delta H_0} \quad \text{(eq.3)} \quad \text{where}$$

- $\frac{dH}{dt}$ is the reaction enthalpy flow measured by photo-DSC
- n is the number of C=C bond per monomer (2 for BEMA)
- m is the moles of monomers in the sample
- ΔH_0 is the standard enthalpy of reaction for the dimethacrylate double bond (56 kJ mol^{-1})[40]

Mechanical properties are determined by Dynamic Mechanical Analysis (DMA) under shearing using a Dynatest Metravib VA 2000 instrument mounted with an oven and a cooling system with liquid nitrogen. Precursor solution is poured into a Teflon mold (50*10 mm, 300 µm thickness) and photo-cured under various radiation intensities. Obtained coupon samples are then tested with a dynamic displacement of 5 µm and an oscillation frequency of 0.1 Hz. Measurements are carried out with a temperature ramp of 2 °C min^{-1} between -120 °C and 150 °C.

3. Results and Discussion

3.1 Thermo-mechanical measurements

The influence of the photo curing radiation intensity is at first studied from a mechanical point of view. An example of a stand-alone gel polymer electrolyte membrane synthesized for Dynamic Mechanical measurements is presented in Figure 2a and related thermograms are presented in Figure 2b. The storage modulus curve of the pristine BEMA cured at 3 mW cm^{-2} exhibits a well defined glass transition with an onset temperature of -50 °C. When the

liquid solution (ionic liquid and lithium salt) is added to the polymer (dash line, 3 mW cm^{-2}), the glass transition temperature of the material decreases (Tg onset -80 °C) revealing the plasticizing effect of the liquid solution. Moreover, the glass transition occurs in a larger temperature range, which can be explained by the presence of two distinct phases (liquid and polymer) having two different glass transition temperatures from -75°C to -25°C. Between -10 °C and 10 °C, GPE traces display the melting of the liquid solution. The rubbery plateau value largely decreases with the addition of liquid solution from 1880 kPa for the pristine BEMA to 122 kPa for the GPE. This loss is in good accordance with the literature since its value is directly correlated to the crosslinking density[45]. When the radiation intensity increases, from 0.1 to 40 mW cm^{-2}, the rubbery plateau value rises from 82 kPa to 182 kPa. These results suggest that the crosslinking density increases with the radiation intensity.

a. 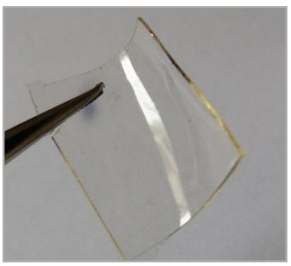

b. 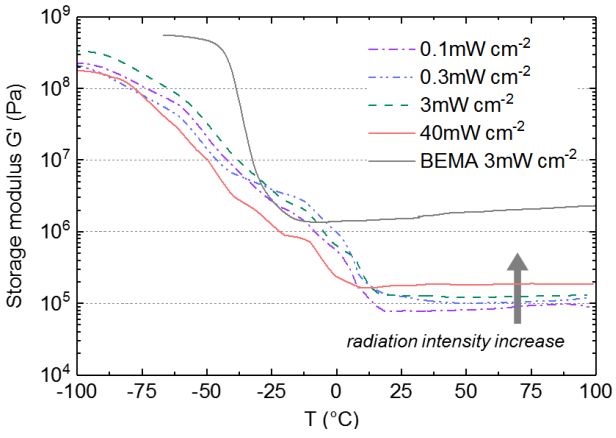

Figure 2: Stand-alone GPE image (a); DMA curves of neat BEMA cured at 3 mW cm^{-2} 60 s and GPE cured at various radiation intensities (b).

To further investigate this phenomenon, the conversion rate of the crosslinking reaction is studied by photo-DSC. The FT-IR spectroscopy, usually used to determine the C=C conversion, is difficult to apply in this case since the relative intensity of the methacrylate

functions bands strongly decreases with the presence of very intense ionic liquid characteristic bands. The conversion rate is then calculated considering the eq.2 and using the reaction enthalpy flow measured by photo-DSC for various radiation intensities (Figure 3a and Figure 3b). It is noteworthy that radiation intensity does not influence the final conversion rate since the conversion is complete in all cases. However, it strongly influences the crosslinking kinetics. For the higher radiation intensities, the conversion rate rapidly increases in the early irradiation stages. It is more obvious on the evolution of the polymerization rate presented in Figure 3c. In the first phase of the reaction, the polymerization rate increases rapidly. This phenomenon, called Trommsdorff effect or autoacceleration, is typically observed for high concentrated methacrylate functions[46]. The viscosity increase of the solution favors the mobility of short molecules. Consequently, free radicals mainly react with monomers, highly concentrated and mobile, rather than with oligomer chains, more cumbersome and thus less mobile. The propagation rate (radicals reacting with monomers) is then higher than the termination one (radicals reacting with already crosslinked polymer parts). After having reached its maximum, the polymerization rate decreases due to the monomers concentration drop. This phase, in which the termination rate is higher than the propagation one, is referred to as autodeceleration. For the highest radiation intensity, both autoacceleration and autodeceleration are fast, indicating that shorter chains are formed considering that the propagation phenomenon is less pronounced. For middle intensity (4 mW cm^{-2}) the curve shape of autodeceleration is smoother, indicating that the propagation phenomenon is more important. In contrast, for low radiation intensity (0.3 mW cm^{-2}), no obvious peak is observed and the polymerization rate remains almost constant during all the irradiation time. This low autoacceleration level indicates that few crosslinking bonds are initiated to the benefit of longer polymer chains.

These assumptions are supported by the evolution of the radiation energy needed to achieve 100 % of conversion reported in Figure 3d. Indeed, this total radiation energy is not constant with the radiation intensity, suggesting that the final structure of the crosslinking polymer is strongly dependent on the radiation intensity and therefore on the crosslinking kinetics. When the radiation intensity increases, the irradiation energy needed to reach 100 % conversion rises from 78 to 225 mJ cm^{-2} for 0.3 and 32 mW cm^{-2} respectively. These results are in good agreement with the assumption that higher radiation intensities lead to shorter polymer chains and higher crosslinking density, which means that the polymer network is less mobile and that remaining radicals will require more energy to move and react.

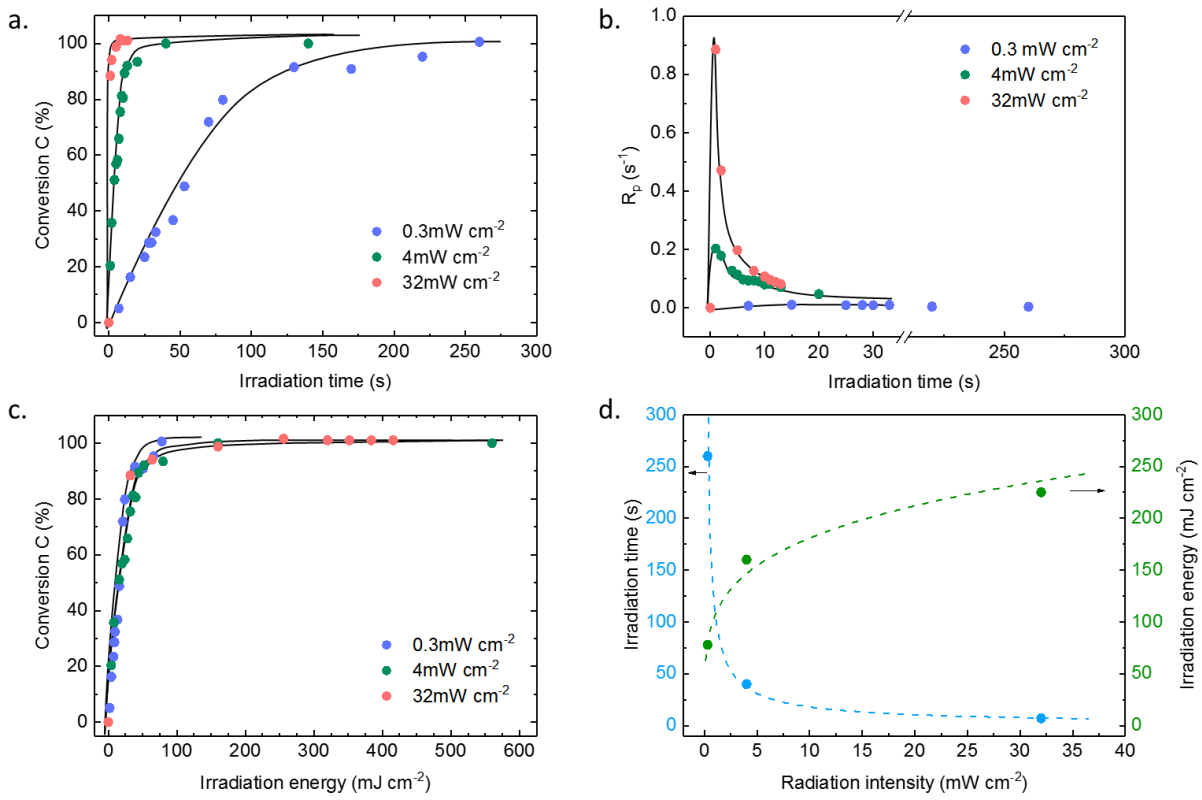

Figure 3: Photo-DSC results for GPE cured at various radiation intensities: conversion rate evolution over irradiation time (a) or radiation energy (b), polymerization rate evolution over irradiation time (c), Irradiation time or energy needed to reach 100 % of conversion rate under various radiation intensities (d), (lines for eye guidance only).

Furthermore, the evolution of the GPE melting peak under various photo-curing conditions gives valuable information on the polymerization kinetic and mechanism. The DSC thermograms of pristine materials are given in supplementary file Figure S2. The melting peak of GPE precursor solution is at about -1 °C, significantly lower than the pristine BEMA (11 °C)[47]. During the photo-polymerization of the neat BEMA (supplementary file Figure S3), the melting peak area, corresponding to the melting enthalpy, decreases until no peak remains after 5 s of irradiation. Additionally, it shifts toward lower temperatures, which can be explained by a decrease of the reactive functions concentration with the polymerization reaction progress. Moreover, the total disappearance of any melting peak shows that the crosslinked polymer is totally amorphous. The melting peak evolution can then be used to follow the crosslinking reaction progress. For the higher radiation intensity (32 mW cm^{-2}, Figure 4), the melting peak area (A) decreases rapidly in the first curing seconds and shifts towards lower temperatures, from -1.3 to -5.7 °C. This peak (A) completely disappears after 2 s which confirms the total conversion of acrylate functions at the end of the irradiation. No other peak is observed which confirms the homogeneity of the precursor solution and a behavior close to the neat BEMA with the formation of an amorphous material. At 4 mW cm^{-2}, the initial curve is slightly different from the other initial ones. The melting temperature is higher (> 0 °C) and the melting peak (A') is larger and asymmetric (spread towards lower temperatures). Compared to DSC thermograms of pristine components (supplementary file Figure S2), the 4 mW.cm^{-2} curve displays the shape of the ionic liquid and Li salt solution[48] rather than the total precursor solution. From 2.5 s, two other peaks (A and B) appear. The first one (A) at lower temperature (-5 °C) remains after 5 s of irradiation while the initial peak A' totally disappears. This melting peak A at -5 °C is similar to the BEMA peak observed at others radiation intensities. After 30 s of irradiation, both A and A' peaks disappear and only

B peak remains. This suggests that A and A' are attributed to the non-polymerized phase and C=C transformation. Two peaks possibly appear due to an inhomogeneous initial solution, maybe caused by an insufficient stirring. The evolution of the melting peaks A and A' with irradiation time suggests that the polymerization kinetic is lower at this radiation intensity. At 0.3 mW cm^{-2}, the initial peak is the expected one (A) proving the good homogeneity of the solution. After 50 s of irradiation, the B peak appears and both A and B peaks are still present even after 203 s. At 400 s, only the B peak remains. This confirms that the kinetic decreases with the radiation intensity. The B peak appearance for the lower radiation intensity confirms that the crosslinking mechanism strongly depends on the radiation intensity and consequently the polymerization kinetic. Considering the previous results obtained by DMA and photo-DSC, we assume that the B peak may be attributed to a crystalline domain formed in softened polymers. When the radiation intensity decreases, the crosslinking density strongly decreases which may lead to longer linear polymer chains. A new order can be expected in these less constrained areas that can lead to a new crystalline phase formation. Further experiments (XRD, Raman spectroscopy, etc.) are undergoing to confirm this assumption. The formation of a new crystalline phase at lower intensities can be detrimental to the electrochemical performance. Indeed, it is well known in the literature, mainly for the very popular PEO polymer[49], that crystalline domains strongly decrease ionic conductivity.

Considering the previous results, in the following discussions, the irradiation time applied for each radiation intensity will correspond to the time needed to achieve 100 % of conversion.

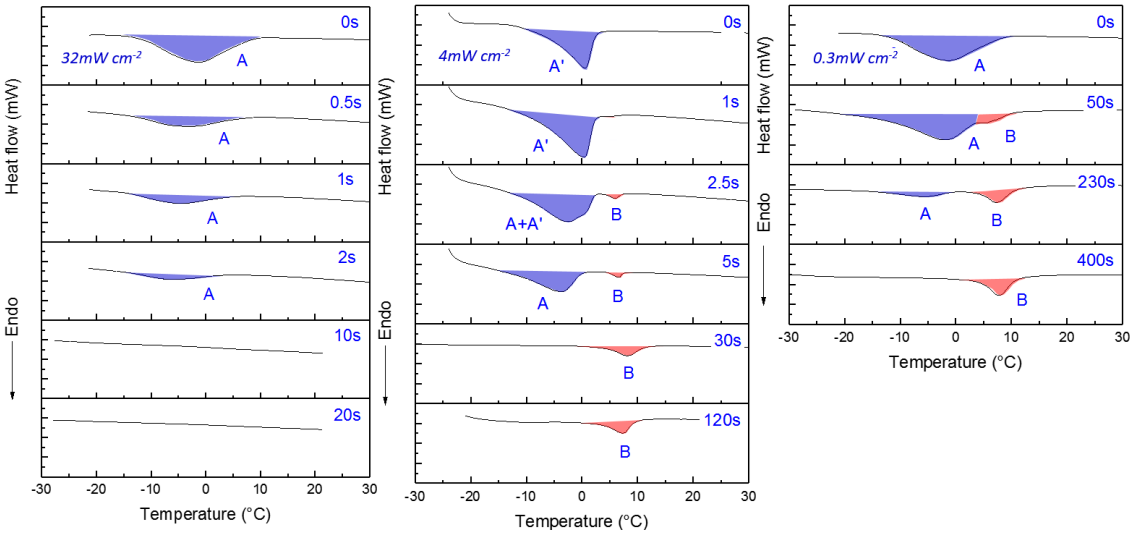

Figure 4: Photo-DSC traces of GPE at various irradiation times for three different radiation intensities.

3.2 Conduction measurements

The temperature dependence of the ionic conductivity for various radiation intensities is presented in Figure 5a. At room temperature, the higher radiation intensities (50 and 3.1 mW cm^{-2}) exhibit similar ionic conductivity of about 0.6 mS cm^{-1}. For the lower radiation intensity (0.7 mW cm^{-2}), the conductivity is slightly higher, up to 0.8 mS cm^{-1}. For any radiation intensities, the Arrhenius plots (log(σ) vs 1000/T) do not exhibit a linear evolution but a curved shape. This is typical of a GPE behavior above Tg and is related to the free volume theory, where the ion mobility depends on the free volume distribution allowing this mobility. Hence, the conductivity can be fitted by the Vogel-Tammann-Fulcher (VTF) equation[5, 50]:

$$\sigma = \frac{A}{\sqrt{T}} \cdot exp\left(\frac{-B}{k_B(T-T_0)}\right) \quad \text{(eq.5)}$$

Where A is a prefactor related to the number of charge carriers (S cm^{-1} $K^{-1/2}$), B is a pseudo-activation energy (J), T_0 (K) is a theoretical glass transition temperature and k_B the Boltzmann constant (1.3806 J K^{-1}). At T_0, the entropy is zero and there is no more free volume. T_0 is typically 20-50 K lower than the glass transition temperature of the host polymer. According to equation 5, the evolution of ln ($\sigma T^{1/2}$) versus 1000/(T-T_0) is plotted in Figure 5b and the fitting parameters are reported in Table 1. The linear fitting confirms the VTF behavior with correlation factors close to 0.99. The two highest radiation intensities (50 and 3.1 mW cm^{-2}) exhibit quite similar behavior with close fitting parameters. The lowest intensity radiation is quite different. At first, the T_0 value largely decreases, from 240 K (-32 °C) to 184 K (-89 °C). This is in good accordance with previous DMA and photo-DSC results, which show a lower rubbery plateau value and lower crosslinking density for 0.7 mW cm^{-2}. The prefactor A, related to the charge carriers number, largely increases at 0.7 mW cm^{-2} meaning that there are more free ions in this polymer structure. However, the pseudo-activation energy B also increases for this lowest radiation intensity. This correlation between the prefactor A and the pseudo-activation energy B is referred in the literature as the compensation effect and have been interestingly studied by Diederichsen *et al*[50] which described a positive linear relationship between ln(A) and B for various electrolyte types (gel, solid, etc.). In our study, we also found a linear relationship between the pseudo-activation energy B and the natural log of the prefactor A with a correlation factor R^2 of 0.951. Even if this observation is weak considering that it is based only on 3 experimental points, it gives interesting information on the conduction mechanism in this GPE. Indeed, the ionic conductivity for the lower radiation intensity increase (0.8 mS cm^{-1}) with the prefactor A and despite the pseudo-activation energy B increase. In solid polymer electrolytes[50], this B factor is often related to the polymer segmental motion. In GPE, it is known that the conduction mechanism is complex and results

from a mix between transport in the liquid phase, segmental chain motion and Li^+ hop assisted by the host polymer[51]. The main impact of the charge carrier number indicates that the conduction mechanism in this GPE is more managed by the transport in the liquid phase than through the polymer backbone (segmental chain motion and Li^+ hop).

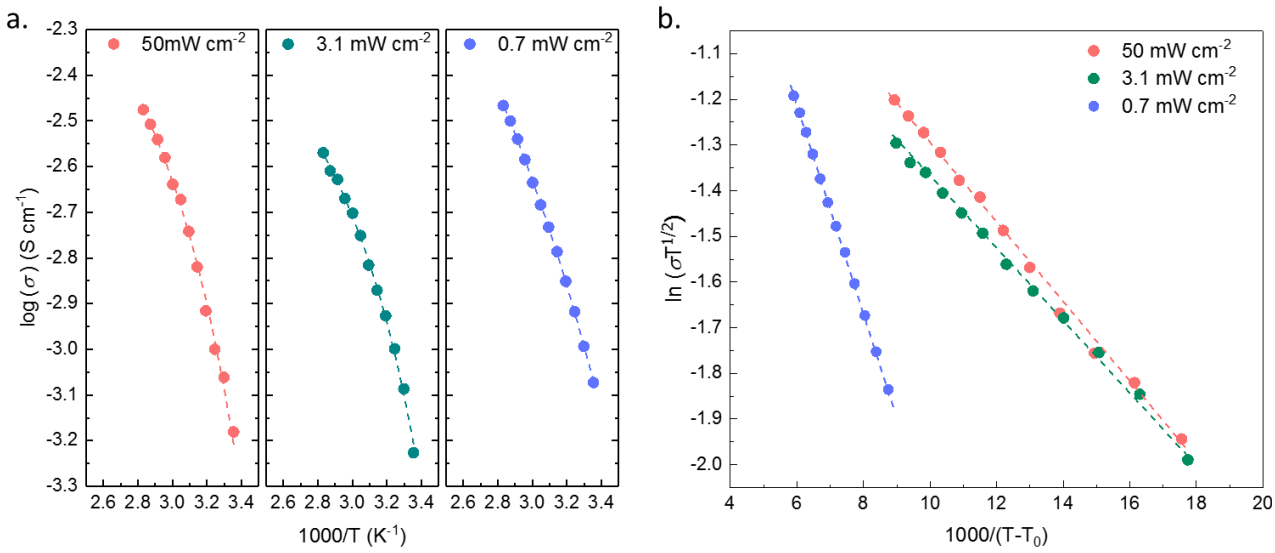

Figure 5: (a) Conductivity-temperature plots of GPE polymerized at various radiation intensities; (b) VTF fitting curves of GPE polymerized at various radiation intensities.

Radiation intensity	$\sigma_{25°C}$ (mS cm^{-1})	VTF parameters			
		A (S cm^{-1} K$^{1/2}$)	B (eV)	T_0 (K)	R^2
50 mW cm^{-2}	0.66	0.4	0.017	241	0.989
3.1 mW cm^{-2}	0.59	0.24	0.015	240	0.990
0.7 mW cm^{-2}	0.83	1.4	0.044	184	0.998

Table 1: Ionic conductivity at 25°C and VTF fitting parameters for each radiation intensity.

The evolution of the diffusion coefficient of each nucleus at 25°C before and after photo-curing is presented in Figure 6a. A large decrease of the diffusion coefficients (40-50 %) is observed for ^{1}H (Pyr) and ^{19}F (TFSI) nuclei. This is consistent with the fact that crosslinking fixes the liquid phase into the host polymer and hence limits the ions mobility. However, the diffusion coefficient of Li largely decreases compared to the other ones of at least two decades. This confirms that the host polymer strongly interacts with Li. As reported in the literature[51], the oxygen atoms of the polymer chains form a complex with lithium. When the host polymer is crosslinked, the oxygen atoms are less mobile and therefore Li are trapped. This result tends to prove that after crosslinking, lithium are more complexed by ethylene oxide chains than by TFSI, otherwise ^{19}F diffusion coefficient should exhibit the same decreasing behavior than the Li one. This evidences the huge influence of the polymer on the Li diffusion. At 60 °C, diffusion coefficients of all nuclei increase and are multiplied by 5 or 6, mainly due to the liquid phase viscosity decrease with the temperature rise. Figure 6b presents the evolution of the diffusion coefficient at 60 °C under various radiation intensities. ^{19}F diffusion coefficient (TFSI) is stable whatever the radiation intensity. ^{1}H diffusion coefficient (Pyr_{13}) is quite stable even if a small decrease is observed at 30 mW cm^{-2}. ^{7}Li

coefficient diffusion (Table 2) varies from 1.9 to 2.3.10^{-13} m^2 s^{-1} with no specific trend according to the curing sequence.

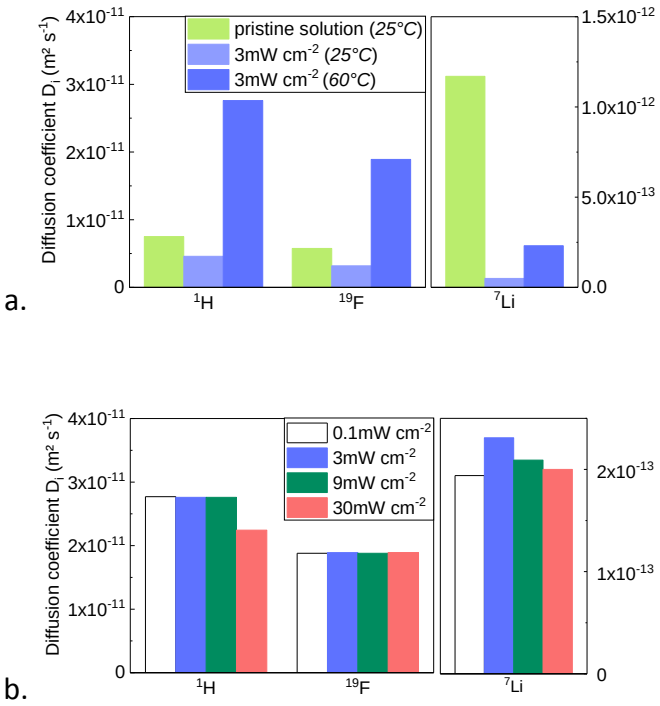

Figure 6: Diffusion coefficient of each nucleus determined by PGSE-NMR spectroscopy (a) before (pristine precursors solution) at 25 °C and after irradiation process (3 mW cm^{-2}) at 25 °C and 60 °C; (b) at 60 °C for GPE cured at various radiation intensities.

This determination of the diffusion coefficients of each nucleus allowed to calculate the Li transference number T_{Li}. There are many debates in the literature on the definition of the transport and transference number and the validity of their determination[52-53]. The transport number is valid in an ideal solution (diluted system) where each ion is perfectly dissociated. However, in concentrated solutions, like GPE and ionic liquids, ions are not totally dissociated and mostly present as ionic associations ($Li[TFSI]_2^-$, $Li_2[TFSI]^+$, etc.) or neutral clusters (Li[TFSI]). As the charge might be transported by all mobile species, it seems more representative to consider in such systems the transference number T_{Li} which takes into account all charged species containing the lithium element:

$$T_{Li} = \alpha t_{Li^+} - \beta t_{LiX_2^-} + \gamma 2 t_{Li_2X^+} + \cdots \text{ (eq.6)}$$

Most popular techniques to determine the transference number are electrochemical methods like the Bruce & Vincent [54] or Watanabe[55-56] experiments. However, these methods, based on the assumption that the contribution of ionic aggregates is negligible (diluted solution), are not strictly transposable for our GPE. Therefore, in this work, we used the diffusion coefficients determined by PFG-NMR technique to evaluate the transference number. This technique presents the benefit to take into account all mobile species. In return, it also considers neutral species which do not contribute to current transport. The T_{Li} value is then slightly overestimated compared to the effective electrochemical one. The transference number of each nucleus can be determined through the diffusion coefficient thanks to the following relation:

$$T_i = \frac{\alpha_i D_i}{\sum_j \alpha_j D_j} \quad \text{(eq.7)}$$

Where α_i is the molar ratio of the i specie and D_i its diffusion coefficient previously determined by PFG-NMR technique.

Radiation intensity	$D_{^7Li}$ (m² s^{-1})	T_{Li}
0.1 mW.cm^{-2}	1.94 .10^{-13}	0.0011
3 mW.cm^{-2}	2.31 .10^{-13}	0.0013
9 mW.cm^{-2}	2.09 .10^{-13}	0.0012
30 mW.cm^{-2}	2.00 .10^{-13}	0.0013

Table 2: Diffusion coefficient and transference number of Li determined by PFG-NMR at 60°C.

The evolution of the T_{Li} for the various radiation intensities is shown in Table 2. No obvious trend with radiation intensity is evidenced and the T_{Li} value is very low (0.0013) mainly due to the host polymer oxygen trapping Li as previously described. The Li conductivity evolution is then only proportional to the total ionic conductivity, which rises with the radiation intensity decrease. However, the very low T_{Li} value means that Li charged species (Li^+, Li_2TFSI^+, etc.) will achieve only a very few portion of the current transport in the battery which could provide various performance decays[57] (poor high current behavior, important concentration gradients, dendritic growth, etc.) as observed in galvanostatic curves (supplementary file Figure S4).

4. Conclusion

Gel polymer electrolyte is prepared through an interesting, solvent free, photoinitiated crosslinking process. The polymerization kinetics are found to be highly dependent on the radiation intensity. The conversion rate reaches 100 % in all cases but with only 7 s of irradiation for 32 mW cm^{-2} while 260 s are needed for 0.3 mW cm^{-2}. The radiation intensity is shown to greatly influence the mechanical strength of the obtained GPE, with a higher shear modulus for the highest radiation intensity (182 kPa). The crosslinking mechanism is highly correlated to the radiation intensity considering the photo-DSC results. Higher radiation intensities tend to form short polymer chains with high crosslinking density while lower radiation intensities form softened polymer with longer chains and fewer crosslinking points. The formation of a new crystalline phase with the radiation intensity decrease is also observed. This structural evolution leads to a rise of the ionic conductivity (up to 0.8 $mS.cm^{-1}$ at 25°C) for the lowest radiation intensity while no obvious difference is detected on the

diffusion coefficients. The Li transference number of the GPE remains very low (0.0013) whatever the curing sequence. Therefore, the low Li transference number of the GPE material on which this study is based on does not allow observing a significant improvement of the electrochemical performance with the curing sequence. However, this study displays promising observations on the curing sequence influence on the polymer structure and the resulting conduction mechanism which should be transposed to optimized GPE material.

Acknowledgements

Authors thank P.A. Bayle (Univ. Grenoble Alpes, CEA, INAC-MEM, LRM, MINATEC Campus) for technical expertise and fruitful discussions on PFG-NMR measurements.

Financial support for this work was provided through the EnSO project. EnSO has been accepted for funding within the Electronic Components and Systems For European Leadership Joint Undertaking in collaboration with the European Union's H2020 Framework Program (H2020/2014-2020) and National Authorities, under grant agreement n° 692482.

References

(1) Armand, M., The history of polymer electrolytes. *Solid State Ionics* **1994,** *69* (3), 309-319.

(2) Berthier, C.; Gorecki, W.; Minier, M.; Armand, M. B.; Chabagno, J. M.; Rigaud, P., Microscopic investigation of ionic conductivity in alkali metal salts-poly(ethylene oxide) adducts. *Solid State Ionics* **1983,** *11* (1), 91-95.

(3) M. Armand, J. M. C., M. Duclot In *Polymeric solid electrolytes*, Second International Meeting on Solid Electrolytes, St. Andrews, Scotland, St. Andrews, Scotland, 1978.

(4) Dias, F. B.; Plomp, L.; Veldhuis, J. B. J., Trends in polymer electrolytes for secondary lithium batteries. *J. Power Sources* **2000,** *88* (2), 169-191.

(5) Mindemark, J.; Lacey, M. J.; Bowden, T.; Brandell, D., Beyond PEO—Alternative host materials for Li+-conducting solid polymer electrolytes. *Prog. Polym. Sci.* **2018,** *81*, 114-143.

(6) Guo, H.-L.; Sun, H.; Jiang, Z.-L.; Luo, C.-S.; Gao, M.-Y.; Wei, M.-H.; Hu, J.-Y.; Shi, W.-K.; Cheng, J.-Y.; Zhou, H.-J., A new type of composite electrolyte with high performance for room-temperature solid-state lithium battery. *Journal of Materials Science* **2018**.

(7) Zhao, H.; Jia, Z.; Yuan, W.; Hu, H.; Fu, Y.; Baker, G. L.; Liu, G., Fumed Silica-Based Single-Ion Nanocomposite Electrolyte for Lithium Batteries. *ACS Appl. Mater. Interfaces* **2015,** *7* (34), 19335-19341.

(8) Hu, J.; Wang, W.; Peng, H.; Guo, M.; Feng, Y.; Xue, Z.; Ye, Y.; Xie, X., Flexible Organic–Inorganic Hybrid Solid Electrolytes Formed via Thiol–Acrylate Photopolymerization. *Macromolecules* **2017,** *50* (5), 1970-1980.

(9) Feuillade, G.; Perche, P., Ion-conductive macromolecular gels and membranes for solid lithium cells. *J. Appl. Electrochem.* **1975,** *5* (1), 63-69.

(10) Cheng, X.; Pan, J.; Zhao, Y.; Liao, M.; Peng, H., Gel Polymer Electrolytes for Electrochemical Energy Storage. *Adv. Energy Mater.* **2018,** *8* (7).

(11) Chen, S.; Wen, K.; Fan, J.; Bando, Y.; Golberg, D., Progress and future prospects of high-voltage and high-safety electrolytes in advanced lithium batteries: from liquid to solid electrolytes. *Journal of Materials Chemistry A* **2018,** *6* (25), 11631-11663.

(12) Kalhoff, J.; Eshetu, G. G.; Bresser, D.; Passerini, S., Safer Electrolytes for Lithium-Ion Batteries: State of the Art and Perspectives. *ChemSusChem* **2015,** *8* (13), 2154-2175.

(13) Tarascon, J. M.; Gozdz, A. S.; Schmutz, C.; Shokoohi, F.; Warren, P. C., Performance of Bellcore's plastic rechargeable Li-ion batteries. *Solid State Ionics* **1996,** *86-88*, 49-54.

(14) He, R.; Kyu, T., Effect of Plasticization on Ionic Conductivity Enhancement in Relation to Glass Transition Temperature of Crosslinked Polymer Electrolyte Membranes. *Macromolecules* **2016,** *49* (15), 5637-5648.

(15) Noda, A.; Watanabe, M., Highly conductive polymer electrolytes prepared by in situ polymerization of vinyl monomers in room temperature molten salts. *Electrochim. Acta* **2000,** *45* (8), 1265-1270.

(16) Yang, P.; Liu, L.; Li, L.; Hou, J.; Xu, Y.; Ren, X.; An, M.; Li, N., Gel polymer electrolyte based on polyvinylidenefluoride-co-hexafluoropropylene and ionic liquid for lithium ion battery. *Electrochim. Acta* **2014,** *115*, 454-460.

(17) Fernicola, A.; Weise, F. C.; Greenbaum, S. G.; Kagimoto, J.; Scrosati, B.; Soleto, A., Lithium-Ion-Conducting Electrolytes: From an Ionic Liquid to the Polymer Membrane. *J. Electrochem. Soc.* **2009,** *156* (7), A514-A520.

(18) Nair, J. R.; Porcarelli, L.; Bella, F.; Gerbaldi, C., Newly Elaborated Multipurpose Polymer Electrolyte Encompassing RTILs for Smart Energy-Efficient Devices. *ACS Appl. Mater. Interfaces* **2015,** *7* (23), 12961-12971.

(19) Sotta, D.; Bernard, J.; Sauvant-Moynot, V., Application of electrochemical impedance spectroscopy to the study of ionic transport in polymer-based electrolytes. *Prog. Org. Coat.* **2010,** *69* (2), 207-214.

(20) Rymarczyk, J.; Carewska, M.; Appetecchi, G. B.; Zane, D.; Alessandrini, F.; Passerini, S., A novel ternary polymer electrolyte for LMP batteries based on thermal cross-linked poly(urethane acrylate) in presence of a lithium salt and an ionic liquid. *Eur. Polym. J.* **2008,** *44* (7), 2153-2161.

(21) Gerbaldi, C.; Nair, J. R.; Ahmad, S.; Meligrana, G.; Bongiovanni, R.; Bodoardo, S.; Penazzi, N., UV-cured polymer electrolytes encompassing hydrophobic room temperature ionic liquid for lithium batteries. *J. Power Sources* **2010,** *195* (6), 1706-1713.

(22) Rupp, B.; Schmuck, M.; Balducci, A.; Winter, M.; Kern, W., Polymer electrolyte for lithium batteries based on photochemically crosslinked poly(ethylene oxide) and ionic liquid. *Eur. Polym. J.* **2008,** *44* (9), 2986-2990.

(23) Kim, G. T.; Appetecchi, G. B.; Carewska, M.; Joost, M.; Balducci, A.; Winter, M.; Passerini, S., UV cross-linked, lithium-conducting ternary polymer electrolytes containing ionic liquids. *J. Power Sources* **2010,** *195* (18), 6130-6137.

(24) Nair, J. R.; Colò, F.; Kazzazi, A.; Moreno, M.; Bresser, D.; Lin, R.; Bella, F.; Meligrana, G.; Fantini, S.; Simonetti, E.; Appetecchi, G. B.; Passerini, S.; Gerbaldi, C., Room temperature ionic liquid (RTIL)-based electrolyte cocktails for safe, high working potential Li-based polymer batteries. *J. Power Sources* **2019,** *412*, 398-407.

(25) Abdelhedi-Miladi, I.; Montarnal, D.; Obadia, M. M.; Ben Romdhane, H.; Drockenmuller, E., UV-Patterning of Ion Conducting Negative Tone Photoresists Using Azide-Functionalized Poly(Ionic Liquid)s. *ACS Macro Letters* **2014,** *3* (11), 1187-1190.

(26) Wang, S.; Liu, X.; Wang, A.; Wang, Z.; Chen, J.; Zeng, Q.; Jiang, X.; Zhou, H.; Zhang, L., High-Performance All-Solid-State Polymer Electrolyte with Controllable Conductivity Pathway Formed by Self-Assembly of Reactive Discogen and Immobilized via a Facile Photopolymerization for a Lithium-Ion Battery. *ACS Appl. Mater. Interfaces* **2018,** *10* (30), 25273-25284.

(27) Odian, G., *Principles of Polymerization, 4th edition*. 2004.

(28) Li, Z.; Jiang, J.; Lei, G.; Gao, D., Gel polymer electrolyte prepared by in situ polymerization of MMA monomers in room temperature ionic liquid. *Polym. Adv. Technol.* **2006,** *17* (7-8), 604-607.

(29) Hermosilla, L.; Calle, P.; Tiemblo, P.; García, N.; Garrido, L.; Guzmán, J., Polymerization of Methyl Methacrylate with Lithium Triflate. A Kinetic and Structural Study. *Macromolecules* **2013,** *46* (14), 5445-5454.

(30) Kil, E. H.; Choi, K. H.; Ha, H. J.; Xu, S.; Rogers, J. A.; Kim, M. R.; Lee, Y. G.; Kim, K. M.; Cho, K. Y.; Lee, S. Y., Imprintable, bendable, and shape-conformable polymer electrolytes for versatile-shaped lithium-ion batteries. *Adv. Mater.* **2013,** *25* (10), 1395-1400.

(31) Kim, S. H.; Choi, K. H.; Cho, S. J.; Park, J. S.; Cho, K. Y.; Lee, C. K.; Lee, S. B.; Shim, J. K.; Lee, S. Y., A shape-deformable and thermally stable solid-state electrolyte based on a plastic crystal composite polymer electrolyte for flexible/safer lithium-ion batteries. *Journal of Materials Chemistry A* **2014,** *2* (28), 10854-10861.

(32) Gerbaldi, C.; Nair, J. R.; Meligrana, G.; Bongiovanni, R.; Bodoardo, S.; Penazzi, N., Highly ionic conducting methacrylic-based gel-polymer electrolytes by UV-curing technique. *J. Appl. Electrochem.* **2009,** *39* (11), 2199-2207.

(33) Echeverri, M.; Hamad, C.; Kyu, T., Highly conductive, completely amorphous polymer electrolyte membranes fabricated through photo-polymerization of poly(ethylene glycol diacrylate) in mixtures of solid plasticizer and lithium salt. *Solid State Ionics* **2014,** *254*, 92-100.

(34) Ravve, A., *Principles of polymer chemistry, third edition*. 2012.

(35) Kaczmarek, H.; Vuković-Kwiatkowska, I., Preparation and characterization of interpenetrating networks based on polyacrylates and poly(lactic acid). *Express Polymer Letters* **2012,** *6* (1), 78-94.

(36) Chiappone, A.; Nair, J. R.; Gerbaldi, C.; Bongiovanni, R.; Zeno, E., UV-cured Al2O3-laden cellulose reinforced polymer electrolyte membranes for Li-based batteries. *Electrochim. Acta* **2015,** *153*, 97-105.

(37) Tosoni, M.; Schulz, M.; Hanemann, T., Novel conductive gel polymers based on acrylates and ionic liquids. *Int. J. Electrochem. Sci.* **2014,** *9* (7), 3602-3617.

(38) Jin, M.; Zhang, Y.; Yan, C.; Fu, Y.; Guo, Y.; Ma, X., High-Performance Ionic Liquid-Based Gel Polymer Electrolyte Incorporating Anion-Trapping Boron Sites for All-Solid-State Supercapacitor Application. *ACS Appl. Mater. Interfaces* **2018,** *10* (46), 39570-39580.

(39) Imperiyka, M.; Ahmad, A.; Hanifah, S. A.; Rahman, M. Y. A., Potential of UV-curable poly(glycidyl methacrylate-co-ethyl methacrylate)-based solid polymer electrolyte for lithium ion battery application. *Int. J. Electrochem. Sci.* **2013,** *8* (9), 10932-10945.

(40) Dean, K.; Cook, W. D., Effect of Curing Sequence on the Photopolymerization and Thermal Curing Kinetics of Dimethacrylate/Epoxy Interpenetrating Polymer Networks. *Macromolecules* **2002,** *35* (21), 7942-7954.

(41) Hahn, E. L., Spin Echoes. *Physical Review* **1950,** *80* (4), 580-594.

(42) Stejskal, E. O.; Tanner, J. E., Spin Diffusion Measurements: Spin Echoes in the Presence of a Time-Dependent Field Gradient. *The Journal of Chemical Physics* **1965,** *42* (1), 288-292.

(43) Tanner, J. E.; Stejskal, E. O., Restricted Self-Diffusion of Protons in Colloidal Systems by the Pulsed-Gradient, Spin-Echo Method. *The Journal of Chemical Physics* **1968,** *49* (4), 1768-1777.

(44) Price, W. S., Pulsed-field gradient nuclear magnetic resonance as a tool for studying translational diffusion: Part 1. Basic theory. *Concepts in Magnetic Resonance* **1997,** *9* (5), 299-335.

(45) Mammeri, F.; Le Bourhis, E.; Rozes, L.; Sanchez, C., Mechanical properties of hybrid organic-inorganic materials. *J. Mater. Chem.* **2005,** *15* (35-36), 3787-3811.

(46) Anseth, K. S.; Wang, C. M.; Bowman, C. N., Reaction behaviour and kinetic constants for photopolymerizations of multi(meth)acrylate monomers. *Polymer* **1994,** *35* (15), 3243-3250.

(47) Ceccorulli, G., Zini, E. and Scandola, M. , Study of Organic Phase Mobility in Nanocomposite Organic-Inorganic Coatings. *Macromol. Chem. Phys.* **2006,** *207* (10), 864-869.

(48) Henderson, W. A.; Passerini, S., Phase Behavior of Ionic Liquid−LiX Mixtures: Pyrrolidinium Cations and TFSI- Anions. *Chem. Mater.* **2004,** *16* (15), 2881-2885.

(49) Commarieu, B.; Paolella, A.; Daigle, J.-C.; Zaghib, K., Toward high lithium conduction in solid polymer and polymer–ceramic batteries. *Current Opinion in Electrochemistry* **2018,** *9*, 56-63.

(50) Diederichsen, K. M.; Buss, H. G.; McCloskey, B. D., The Compensation Effect in the Vogel–Tammann–Fulcher (VTF) Equation for Polymer-Based Electrolytes. *Macromolecules* **2017,** *50* (10), 3831-3840.

(51) Meyer, W. H., Polymer Electrolytes for Lithium-Ion Batteries. *Adv. Mater.* **1998,** *10* (6), 439-448.

(52) Lewandowski, A.; Świderska-Mocek, A., Ionic liquids as electrolytes for Li-ion batteries—An overview of electrochemical studies. *J. Power Sources* **2009,** *194* (2), 601-609.

(53) Galiński, M.; Lewandowski, A.; Stępniak, I., Ionic liquids as electrolytes. *Electrochim. Acta* **2006,** *51* (26), 5567-5580.

(54) Bruce, P. G.; Evans, J.; Vincent, C. A., Conductivity and transference number measurements on polymer electrolytes. *Solid State Ionics* **1988,** *28-30*, 918-922.

(55) Watanabe, M.; Nagano, S.; Sanui, K.; Ogata, N., Estimation of Li+ transport number in polymer electrolytes by the combination of complex impedance and potentiostatic polarization measurements. *Solid State Ionics* **1988,** *28-30*, 911-917.

(56) Hiller, M. M.; Joost, M.; Gores, H. J.; Passerini, S.; Wiemhöfer, H. D., The influence of interface polarization on the determination of lithium transference numbers of salt in polyethylene oxide electrolytes. *Electrochim. Acta* **2013,** *114*, 21-29.

(57) Diederichsen, K. M.; McShane, E. J.; McCloskey, B. D., Promising Routes to a High Li+ Transference Number Electrolyte for Lithium Ion Batteries. *ACS Energy Letters* **2017,** *2* (11), 2563-2575.